

---

# Enforcing Topological Interaction between Implicit Surfaces via Uniform Sampling

---

**Hieu Le**  
CVLab, EPFL  
minh.le@epfl.ch

**Nicolas Talabot**  
CVLab, EPFL  
nicolas.talabot@epfl.ch

**Jiancheng Yang**  
CVLab, EPFL  
jiancheng.yang@epfl.ch

**Pascal Fua**  
CVLab, EPFL  
pascal.fua@epfl.ch

## Abstract

Objects interact with each other in various ways, including containment, contact, or maintaining fixed distances. Ensuring these topological interactions is crucial for accurate modeling in many scenarios. In this paper, we propose a novel method to refine 3D object representations, ensuring that their surfaces adhere to a topological prior. Our key observation is that the object interaction can be observed via a stochastic approximation method: the statistic of signed distances between a large number of random points to the object surfaces reflect the interaction between them. Thus, the object interaction can be indirectly manipulated by using choosing a set of points as anchors to refine the object surfaces. In particular, we show that our method can be used to enforce two objects to have a specific contact ratio while having no surface intersection. The conducted experiments show that our proposed method enables accurate 3D reconstruction of human hearts, ensuring proper topological connectivity between components. Further, we show that our proposed method can be used to simulate various ways a hand can interact with an arbitrary object.

## 1 Introduction

Modeling the interaction between objects is at the heart of numerous applications such as computer graphics, virtual reality, robotics, and health care. Most existing works focus on the dynamic interactions between human objects such as hand-object [21], body-garment [16], or human-scene [6]. In this paper, we focus on the problem of multi-objects reconstruction where there is a strong prior indicating the topological interaction between them. The goal is to simultaneously reconstruct multiple objects while ensuring their interaction aligns with a prior. The interaction [4] can take various forms including containment, contact with specific surface ratios, or maintaining fixed distances between objects. This is particularly useful in modeling different parts of composite objects. For example, when reconstructing a heart from imagery for medical purposes, the four ventricles should touch each other at the anatomically appropriate locations, and exhibit the right connections to allow blood flow, but without ever overlapping with each other.

We propose a novel way to enforce topological constraints between 3D objects, with a specific focus on cases like the aforementioned heart ventricles. More specifically, given two 3D objects represented by their deep implicit signed distance functions [19] and a prior indicating a desired contact ratio (%) between them, our goal is to refine them such that they contact each other with that exact ratio and do not intersect. To achieve this, we first uniformly sample a large number of points and compute their signed distances to the two objects. At any given state of the objects, we can estimate the intersection

volume by counting the number of random points that fall within both objects. Similarly, the contact ratio can be estimated by evaluating the ratio of points that lie in close proximity to the surfaces of both objects. Based on the prior, we can estimate the expected number of random points that should be in contact with both objects and fine-tune the object’s implicit functions accordingly.

We apply our proposed method to the problem of reconstructing different components of the 3D human heart. Each pair of heart components exhibits a consistent type of topological interaction. They should never intersect and consistently maintain a specific contact ratio, i.e., there should be no inter-penetrations but they should match tightly, without unwarranted gaps. While these constraints are not automatically satisfied when using individual deepSDF [19] to model each component, the results of our method exhibit proper topological interactions and also have lower Chamfer distances than the baseline method. Further, we show that our proposed system can modify a generative implicit hand model to interact with an arbitrary object in a proper manner. Our proposed losses enable the hand model to be re-positioned and its pose optimized to increase the contact ratio while preventing any intersection with the object.

In short, our core contribution is to show that topological interactions between 3D objects can be enforced via uniformly sampled 3D points. In essence, we use the statistics of random-point-object distances to indirectly observe and manipulate the object interaction.

## 2 Related Work

**Image-Based Topological Interaction.** Many 2D segmentation problems involve semantic classes that have some relative topology constraints between them, such as road connectivity over a background or cell nuclei that should be contained within the cytoplasm. Mosinska et al. [17] proposes a topology-aware loss that uses the response of selected filters from a pre-trained VGG19 network. These filters prefer elongated shapes and thus alleviate the broken connection issue. Hu et al. [9] uses a topology loss based on persistent diagrams to help cell segmentation. Other works rely on detecting and penalizing critical pixels for topology interaction between classes, such as Hu [8] and Gupta et al. [4], using homotopy warping and convolutions respectively to find these pixels. However, image and pixel based topology constraints do not lend themselves easily to implicit multi-object 3D reconstruction.

**Multi-Object 3D Reconstruction.** Multi-object 3D reconstruction [10, 14] is a fundamental task for scene understanding or generation. The presence of multiple objects poses a different set of challenges compared to single-object reconstruction where objects are usually treated as isolated geometries without considering the scene context, such as object locations and instance-to-instance interactions. For multi-object reconstruction, Mesh R-CNN [3] augments Mask R-CNN [7] with a mesh predictions branch that estimates a 3D mesh for each detected object in an image. Total3DUnderstanding [18] presents a framework that predicts room layout, 3D object bounding boxes, and meshes for all objects in an image based on the known 2D bounding boxes. However, these three methods first detect objects in the 2D image, and then independently produce their 3D shapes with single object reconstruction modules. Liu and Liu [14] propose a system to infer the pose, size, and location of 3D bounding boxes and the 3D shapes of multiple object instances in the scene, which is divided into a grid whose cells are occupied by objects. Irshad et al. [11] recovers objects shape, appearance, and poses using implicit representations, as has become increasingly frequent, e.g., [11, 12, 21, 1].

**3D Interaction.** While some works aim to enforce physical plausibility between objects in a scene, e.g., Engelmann et al. [2] that enforces a collision loss between reconstructed objects, most works focus on human-object interactions. Karunratanakul et al. [12] models the grasp between the hand and an object as implicit surfaces and learns to generate new grasps using a VAE, Ye et al. [21] reconstruct from an image the hand-object interaction, and at the same time the object as an implicit surface, and Contact2Grasp [13] learns to synthesize grasps by first predicting a contact map on the object surfaces. Other directions include body-garment interaction, such as DrapeNet [1] with a physically based self-supervision, or human-scene interaction [6]. However, these works primarily focus on interactions between the articulated human body and objects, without incorporating any prior information on how they should interact. In contrast, our approach considers a specific topological prior that needs to be enforced between two objects.

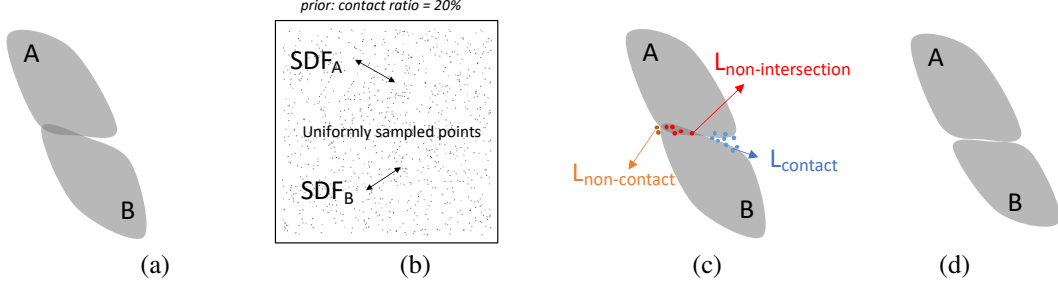


Figure 1: **Overview.** We start with a pair of objects represented by their deep signed distance functions [19] (a) and a prior indicating the desired contact surface percentage. We first compute the signed distances between the two objects and a set of uniformly sampled points (b). We select a subset of points that reside in close proximity to the surfaces of both objects, with the number of points determined based on the provided prior. By utilizing these points as anchors, we refine the objects by fine-tuning their deep-signed distance functions to ensure that no points are located inside the surfaces of both objects while simultaneously pulling the objects towards areas that should be in contact (c). After fine-tuning, the two objects exhibit proper interaction, aligning with the topological prior (d).

### 3 Method

Our method refines two 3D implicit objects to ensure their interaction aligns with a topological prior. In this section, we describe our method designed to enforce two conditions: 1) objects should not intersect each other and 2) they contact each other with given percentage surface areas. Different configurations of our method designed for other interactions are included in the supplementary material.

Figure 1 summarizes our proposed method. Given a pair of objects represented by their deep signed distance functions (deep-SDF)[19] and a prior indicating the contact ratio (the percentage of surface areas that should be in contact with the other object), we first compute the signed distances between the two objects and a randomly sampled point cloud. We then select a subset of points that reside in close proximity to the surfaces of both objects, with the number of points determined based on the provided prior. By utilizing these points as anchors, we refine the objects by fine-tuning their deep-SDF to ensure that no points are located inside the surfaces of both objects while simultaneously pulling the object surfaces towards areas that should be in contact.

#### 3.1 Deep-SDF Preliminary

Implicit surface representations in the form of signed-distance functions [19] have recently emerged as a powerful model to learn continuous representations of 3D shapes. They allow detailed reconstructions of object instances as well as meaningful interpolations between them. A signed distance function of an object is a function that outputs the point’s distance to the closest object surface:

$$SDF(x) = s : x \in \mathbb{R}^3, s \in \mathbb{R} \quad (1)$$

Conventionally, the distance is negative if the point is inside the object and positive otherwise.

In this paper, we focus on the interaction between a pair of objects instances of two categories  $(A, B)$  represented by two deep signed-distance functions  $f_A(a, x) = SDF_A^{idx(a)}(x)$  and  $f_B(b, x) = SDF_B^{idx(b)}(x)$ . Here,  $f_A(\cdot, \cdot)$  and  $f_B(\cdot, \cdot)$  are two deep networks approximating SDFs of multiple objects of category  $A$  and  $B$ , respectively. The latent vector  $a$  encodes information for a specific instance  $idx(a)$  of category  $A$  and the latent  $b$  for a specific object  $idx(b)$  similarly. Following [19],  $f_A(\cdot, \cdot)$  and  $f_B(\cdot, \cdot)$  are trained on a large set of training instances while at test time, we optimize the latent codes  $(a, b)$  based on the testing instances’ signed distances as well as their interaction prior. For the rest of the paper, we refer to the approximated deep SDF functions  $f_A(a, \cdot)$  and  $f_B(b, \cdot)$  as deep-SDF objects.

### 3.2 Enforcing Topological Interaction via Random Points

Let us consider explicit meshes of two 3D objects denoted as  $(M_A, M_B)$ . The contact ratio of mesh  $M_A$  w.r.t. mesh  $M_B$  is defined as follows:

$$P_{M_A, M_B} = \frac{\text{Area}(S_{AB})}{\text{Area}(S_A)} \quad (2)$$

where  $S_{AB}$  represents the partial surface of object  $A$  that includes all points within a small distance to object  $B$ , and  $S_A$  refers to the entire surface of object  $A$ . However, computing this ratio using object meshes is computationally expensive, and further, it is not directly applicable for implicitly represented objects where the object surfaces are not readily available [15]. To overcome this issue, our key observation is that the contact ratio between the two implicit objects can be closely approximated via the signed distances between them to a larger number of uniformly random points. In particular, the contact ratio of a deep-SDF object  $f_A(a_i, \cdot)$  to another deep-SDF object  $f_B(b_i, \cdot)$  can be approximated by the following equation:

$$P'_{A,B} = \frac{\sum_{i=1}^N \mathbb{1}(|f_A(a, x_i)| < \epsilon) \times \mathbb{1}(|f_B(b, x_i)| < \epsilon)}{\sum_{i=1}^N \mathbb{1}(|f_A(a, x_i)| < \epsilon)} \quad (3)$$

where  $\{x_i : i \in (1, N)\}$  is the set of  $N$  uniformly random points,  $\epsilon$  is a small threshold indicating the “contact” distance, and  $\mathbb{1}(\cdot)$  is the indicator function that returns the value 1 if its statement is true and 0 otherwise. In essence, the contact ratio here is estimated via a stochastic Monte Carlo method by counting the number of points lying close to the surfaces of both objects and the number of points lying close to the surface of one object. Our analysis shows that with a large enough value of  $N$ , the result obtained from equation 3 closely approximates the contact ratio calculated using explicit meshes in equation 2.

Building on this observation, we propose to refine the topological interaction between two implicit objects by adjusting their distances to a uniformly sampled point cloud. The goal of the adjustment is to ensure the two objects interact with a similar contact ratio as a given prior while having no intersection. Let us consider two deep-SDF objects  $f_A(a, \cdot)$  and  $f_B(b, \cdot)$  with a prior that  $k\%$  of  $f_A(a, \cdot)$  surface should be in contact distance with  $f_B(b, \cdot)$ . Here we assume that  $k$  is given or can be trivially computed from the training set. Given  $N$  uniformly random points  $\{x_i : i \in (1, N)\}$ , the number of points that is close to the surface of  $f_A(a, \cdot)$  can be calculated as  $\text{Surface}_A = \sum_{i=1}^N \mathbb{1}(|f_A(a, x_i)| < \epsilon)$ . Based on the prior, the expected number of points lying on the contact surface between the two objects should be  $T = \text{Surface}_A \times k\%$ . Thus, we choose a set of anchor points  $\mathcal{A}_{\text{contact}}$  containing the top  $T$  points with the smallest distance to  $B$  among points lying close to the surface of  $A$ . To prevent the two objects from having a larger contact ratio than the prior, we select a set of anchor points  $\mathcal{A}_{\text{non-contact}}$  containing all points within a contact distance to both objects while not being in  $\mathcal{A}_{\text{contact}}$ .

To ensure that there is no intersection between two objects, we find all anchor points lying inside both  $f_A(a, \cdot)$  and  $f_B(b, \cdot)$  and push their surfaces to these points via a non-intersection loss function:

$$\mathcal{L}_{ni} = \sum_{x \in \mathcal{A}_{\text{contact}} \cup \mathcal{A}_{\text{non-contact}} : (f_A(a, x) < 0) \wedge (f_B(b, x) < 0)} \text{clamp}(|f_A(a, x)|, \delta_1) + \text{clamp}(|f_B(b, x)|, \delta_1) \quad (4)$$

where  $\text{clamp}(\cdot, \delta)$  function restricts a given value between an upper and lower bound  $[-\delta, \delta]$  and  $\delta$  are hyper-parameters of our model.

Since  $f_A(a, x)$  and  $f_B(b, x)$  are both negative, this loss function drives the surface of both objects to be pushed toward these anchor points. To enforce a contact ratio of  $k\%$  between the two objects, we enforce that all chosen anchor points in  $\mathcal{A}_{\text{contact}}$  need to be within small distances to both objects via a contact loss function:

$$\mathcal{L}_{\text{contact}} = \sum_{x \in \mathcal{A}_{\text{contact}} : (f_A(a, x) < 0) \vee (f_B(b, x) < 0)} \text{clamp}(|f_A(x) + f_B(x)|, \delta_2) \quad (5)$$

This loss pushes the surfaces of the two objects closer together. In particular, if  $f_A(a, x) < 0$  and  $f_B(a, x) > 0$ , i.e., the point  $x$  lies inside the surface of object  $f_A(a, \cdot)$ , the loss function will increase

$|f_A(a, x)|$  while decreasing  $|f_B(b, x)|^1$  such that their values closely match. If  $f_A(a, x) > 0$  and  $f_B(b, x) > 0$ , the loss simply pulls the surfaces of both objects to this anchor point.

To prevent the two objects from having a larger contact ratio than the given prior, we push the surface of two objects further away from the anchor points in  $\mathcal{A}_{\text{non-contact}}$  by a pushing loss function:

$$\mathcal{L}_{\text{non-contact}} = \sum_{x \in \mathcal{A}_{\text{non-contact}}} \text{clamp}(-f_A(x) - f_B(x), \delta_3) \quad (6)$$

The loss function to fine-tune the deep-SDFs of the two objects is:

$$\mathcal{L} = \mathcal{L}_{ni} \times \lambda_{ni} + \mathcal{L}_{\text{contact}} \times \lambda_{\text{contact}} + \mathcal{L}_{\text{non-contact}} \times \lambda_{\text{non-contact}} + \mathcal{L}_{\text{data}} \times \lambda_{\text{data}} \quad (7)$$

where  $\mathcal{L}_{\text{data}}$  is the data reconstruction term that regresses the signed distances[19] and  $\lambda$  are controlling parameters. During the optimization process, it is important to note that we periodically sample points to ensure they accurately reflect the current state of the object shapes. Further details regarding the loss functions and the optimization algorithm can be found in the supplementary material.

## 4 Metrics and Experiments

We conduct experiments on the task of 3D heart reconstruction and further demonstrate an application for simulating hands-contacting objects. Following [19], we first train deep SDFs models for different objects on a training set. At test time, we optimize a pair of random latent codes such that the models fit the signed distances to the testing objects’ surfaces.

### 4.1 Measuring Topological Interaction Similarity via Signed Distance Histogram Distance

Comparing object interactions is non-trivial since it is hard to describe. Current metrics for 3D object reconstruction including the intersection-over-union (IoU) or Chamfer distance, for the most part, do not sufficiently characterize the differences between two interactions. Two interactions can have small individual parts’ chamfer distances while being completely distinct such as contacting versus slightly intersecting. To measure the topological similarities between two interactions, we propose the use of signed distance histogram distances. The histogram is computed by dividing the range of signed distances ( $[-1, 1]$  in our paper) into bins and then counting the percentage of surface area that falls into each bin. The histogram considers both the intersection ratio (at bin “<0”) and the contact ratio (the smallest positive bin). In this paper, we set the bin values at  $[-\infty, 0, 0.008, 0.08, 0.8, \infty]$  since all meshes are rendered to the size of  $256^3$  while the signed distances range from -1 to 1. Thus, each pixel corresponds to 0.008 units of distance. The distance between two histograms can be computed by summing the absolute difference at each bin.

### 4.2 3D Heart Reconstruction

Accurate reconstruction of heart substructures is important in the development of clinical applications. Here we are particularly interested in building a 3D model of the human heart that is topologically correct, reflecting the accurate connectivity between different parts of human hearts.

We experiment on the whole-heart segmentation dataset introduced by Zhuang and Shen [22], which includes 120 whole-heart models with 3D segmentation of various parts of the human heart such as the myocardium of left ventricle (M-LV), left atrium (LA), left ventricle (LV), right atrium (RA), and right ventricle (RV). The dataset is split into 100 training instances and 20 testing instances. We first extract connectivity priors in terms of contact ratios between different components of the heart, i.e., the ratio between the area of the contact surface over the total surface area of each part. We visualize different components of a 3D heart model and the contact ratios between them in Figure 2. In plot 2b, we use the data meshes to measure the contact ratios (i.e., equation 2) while in plot 2c, we measure the contact ratios via the signed distances of the meshes to a random point cloud (following equation 3). The values between the two plots are closely matched, showing that we can use a set of random points to measure the contact ratio between two 3D objects. As can be seen, 87.5% of the

<sup>1</sup>In this case,  $|f_A(x)|$  is smaller than  $|f_B(x)|$  or else the two objects would intersect.

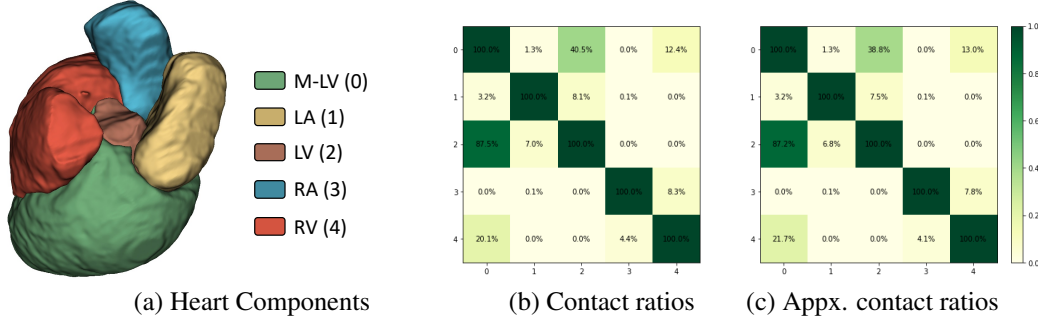


Figure 2: **Different Components of Human Heart and their contact ratios.** We show in (a) a top-down visualization of different components of the human heart: (0) the myocardium of the left ventricle (M-LV), (1) the left atrium (LA), (2) the left ventricle (LV), (3) the right atrium (RA), and (4) the right ventricle (RV). In (b), we show the contact ratios between different components, which is the ratio between the contact surface area over the whole surface area of the object (equation 2). In (c), we show that we can use a set of uniformly random points to closely approximate these ratios (equation 3).

LV’s surface is in contact distance with the M-LV’s surface since M-LV is an outer layer covering LV (see Figure 3). These ratios are relatively consistent across different instances. We average these numbers across the whole training set and use them as priors when reconstructing testing instances.

Table 1 summarizes the results of our method in comparison with deepSDF[19] models trained without our proposed losses. We conduct experiments on different pairs of heart components where we focus on pairs with significant contact ratios: 1) M-LV and LV, 2) LA and LV, 3) RA and RV, and 4) M-LV and RV. We report the average intersection ratio (lower is better), contact ratio (closer to the ground truth is better), chamfer distance (lower is better), and signed distance histogram distance (lower is better). As can be seen, our proposed losses improve the 3D reconstruction in all metrics. The reconstructed components do not intersect each other more than 0.1% in all cases while having contact ratios closely approximating the ground truth. Shapes generated from a vanilla deepSDF [19] model significantly intersect each other while having lower contact ratios.

We visualize qualitative samples for two different cases in Figure 3. For each case, we show how the two heart components connect based on the ground truth data (first two columns), the reconstructed 3D meshes using the baseline method DeepSDF, and the reconstructed 3D meshes using our method. The contact surfaces are colored green while the intersecting surfaces are colored red. The contact and intersection ratios are shown next to the plots. The results of our method show no surface intersection between components. We include more results on whole-heart reconstruction in the supplementary material.

### 4.3 Simulating Hand Contacting Objects

The interaction between human hands and objects poses a significant challenge in modeling, given the variability of hand poses and the diversity of objects involved. Simulating and understanding the various ways in which a hand can come into contact with an object is crucial for numerous applications. We demonstrate that our system using random points to drive the interaction between 3D objects can be used to manipulate a generative hand model to increase the contact ratio between the hand and the object while preventing intersection between them.

We first train an auto-decoder model <sup>2</sup> on the SMPL-H dataset [20] containing 1581 hand meshes captured from 31 subjects, each with 51 hand poses (the same for all subjects). Given the trained hand model and a 3D object in space, we are interested in simulating how a hand interacts with the object. To move the hand in space such that it gets closer to the object, we incorporate an affine transformation consisting of a rotation matrix and a translation vector into the deepSDF model:

$$T(f, z, x, R, r) = f(z, Rx + r) \quad (8)$$

<sup>2</sup>The detailed network architecture and training losses are included in the supplementary material.

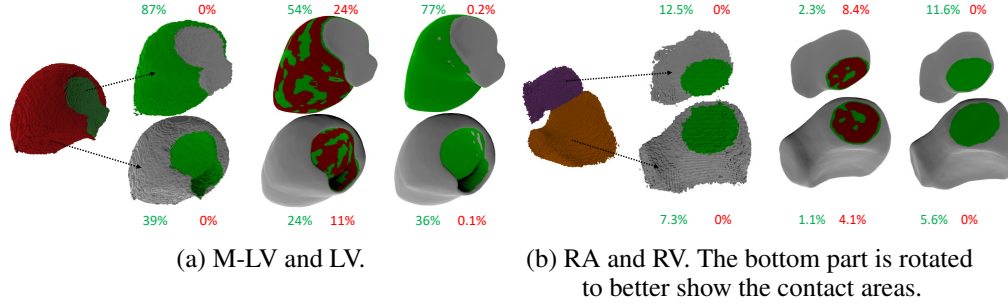


Figure 3: **Refining topological interaction.** We show two cases of how pairs of heart components connect: (a) the myocardium of the left ventricle (M-LV) and the left ventricle (LV) and (b) the right atrium (RA) and the right ventricle (RV). From left to right: the ground-truth 3D meshes, the reconstructed meshes using the baseline method DeepSDF, and the reconstructed 3D meshes using our method. The contact surfaces are colored green while the intersecting surfaces are colored red. The contact and intersection ratios are shown next to the plots.

Table 1: **Heart reconstruction.** We report the average intersection ratio (lower is better), contact ratio (closer to the ground truth is better), chamfer distance (lower is better), and signed distance histogram distance (lower is better). Our proposed losses improve the 3D reconstruction in all metrics where the reconstructed components do not intersect each other more than 0.1% in all cases while having contact ratios closely approximating the ground truth. Shapes generated from a vanilla deepSDF [19] model significantly intersect each other while having lower contact ratios.

Dataset	Part	Intersection (%)		Contact (%)			Chamfer ( $\times 10e4$ )		SDH Dist.	
		dSDF	Ours	GT	dSDF	Ours	dSDF	Ours	dSDF	Ours
MLV-LV	MLV	24.0	0.0	38.6	11.3	35.7	<b>1.4</b>	1.5	1.90	<b>0.31</b>
	LV	53.5	0.1	85.2	24.7	78.3	<b>1.1</b>	<b>1.1</b>		
LA-LV	LA	6.9	0.1	13.0	3.2	9.2	1.6	<b>1.5</b>	0.38	<b>0.12</b>
	LV	4.5	0.1	8.8	2.1	6.1	1.1	<b>1.0</b>		
RA-RV	RA	7.0	0.0	12.8	2.7	8.7	1.6	<b>1.4</b>	0.37	<b>0.14</b>
	RV	3.9	0.0	7.4	1.5	4.8	1.3	<b>1.2</b>		
MLV-RV	RA	8.0	0.0	14.0	3.9	10.9	1.4	<b>1.3</b>	0.12	<b>0.04</b>
	RV	13.4	0.0	22.8	6.5	18.1	1.4	<b>1.2</b>		
Average		15.2	0.0	25.3	7.0	21.5	1.4	<b>1.3</b>	0.7	<b>0.2</b>

where  $R \in \mathbb{R}^{3 \times 3}$  is a rotation matrix and  $r \in \mathbb{R}^3$  is a translation vector. We construct the rotation matrix from the 3 angular parameters such that it does not include any scaling factor. Function  $T(\cdot)$  allows moving an implicit object freely in space while training on only zero-centered data.

To simulate how a hand interacts with an object, we put the deepSDF model of a hand in random positions in space (defined via the affine parameters  $R, r$ ) and the object is at the origin. The latent code is initialized as a random latent code  $z$  from a random training pose. We set a fixed contact ratio prior for hand and object at  $[0.2]$ , i.e., 20% of the hand surface should be in contact distance. However, we must note that finding a realistic hand pose satisfying the exact prior contact ratio is not possible with the generative deepSDF hand model [12] due to the limited training data. Our system, hence, mainly aims to establish hand-object contact while preventing the intersection between them. In fact, our model can strictly enforce a specific contact ratio between the hand and the object but it results in unrealistic hand surfaces.

Table 2 summarizes the results of our proposed method testing on 10 objects from the HO3D dataset [5]. We average over 10 runs for each object. To evaluate the hand-object interaction, we measure the intersection ratio (%): the ratio between the surface area of the hand that intersects the object over the surface area of the hand; and the contact ratio (%) between the hand and the object. Note

that the object can intersect the hand in its initial starting position. Our losses, optimizing over the values of  $(z, R, r)$ , re-position the hand as well as modify the hand pose to lower the intersection while increasing the contact ratios in all cases.

Table 2: **Hand-Object Interactions** The results of our proposed method tested on 10 objects from the HO3D dataset [5] (averaged over 10 runs). We measure the intersection ratio (%): the ratio between the surface area of the hand that intersects the object over the surface area of the hand; and the contact ratio (%) between the hand and the object. We compare these numbers for the hand in its initial state (Init.), the same hand but at the optimized position and angle (Aff.), and the final optimized hand with optimized latent code (Aff. + Latent). Our losses re-position the hand as well as modify the hand pose to lower the intersection ratios while increasing the contact ratios in all cases.

Item	Intersection(%)			Contact(%)		
	Init.	Aff.	Aff. + Latent	Init.	Aff.	Aff. + Latent
11-Banana	6.8	3.7	1.1	2.1	14.1	15.8
24-Bowl	4.9	4.2	0.4	1.5	8.6	10.7
04-Sug.box	4.9	1.1	0.4	1.3	6.8	7.2
06-M.bottle	4.3	1.1	0.8	1.4	8.4	9.4
35-Drill	8.4	3.3	0.5	2.4	4.8	7.0
37-Scissors	4.0	2.5	0.9	1.2	15.9	18.2
61-FoamBrick	8.4	5.3	0.7	2.7	14.2	17.5
25-Mug	3.8	2.8	0.4	1.2	9.3	11.2
03-C.box	10.9	3.8	0.4	2.4	2.9	4.1
52-L.clamp	3.6	1.2	0.4	1.4	6.9	8.0
Mean	6.0	2.8	<b>0.6</b>	1.7	9.0	<b>10.7</b>

Here we do not aim to generate realistic hand grasps but simply force the hand to interact with objects. In many cases, it simply results in the object resting on the hand. Generating realistic hand-grasping objects is a challenging and active research problem on its own. Nevertheless, our system can generate various feasible and realistic hand-object interactions, as can be seen in Figure 4. For each row, we show the original positions of the hand and object in space, and then three views of the optimized hand. Please see the supplementary material for more results.

In Figure 5, we visualize how our losses optimize hand shapes to have better “grips” on objects. For each pair, we show the original hand pose (colored in gray) overlaid by the optimized hand pose (colored in the skin color), and how the optimized hand interacts with the object. The hand model moves the fingers to positions that increase the contact areas (top row) or to positions that do not intersect the objects (bottom row). It shows that our losses can serve as supervision signals to drive generative shape models in meaningful manners.

## 5 Limitations

There are limitations of our work that can be interesting directions for future work. Computing signed distances from object surfaces to a large number of points can be computationally expensive and might not be trivially applicable to other kinds of surface representations. Here we only consider a fixed topological constraint for a given pair of classes while in practice, they can be in a more dynamic form and can be even hard to estimate. Further, we must note that we indirectly manipulate the object surfaces via stochastic Monte Carlo estimation. There is no guarantee about the correctness of the topological interactions since at no point do we directly measure them.

## 6 Conclusions

We discuss the problem of 3D multiple object reconstruction where a topological prior is given. The prior implies the interaction between objects, which can be in the form of contact ratio. Our key observation is that the object interaction can be observed via a stochastic estimation method by uniformly sampling a large number of points and computing distances between them to the objects.



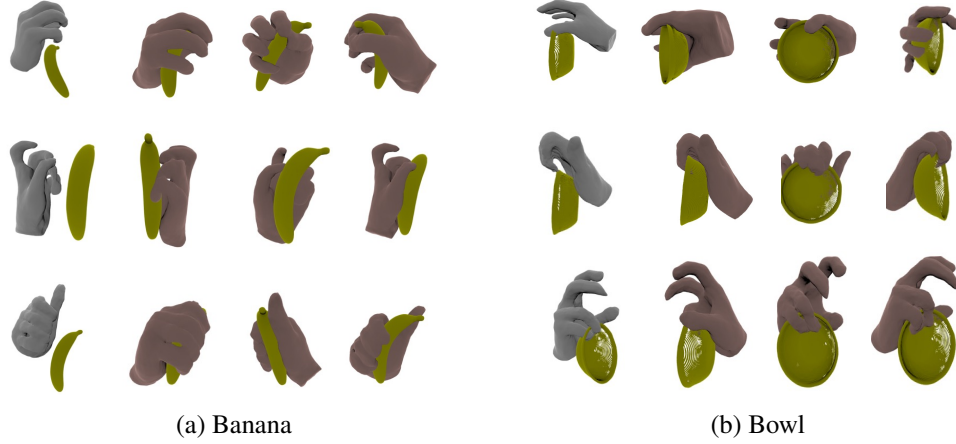


Figure 4: **Generated Hand-Object Interactions.** Our system can generate various feasible and realistic hand-object interactions. The only losses driving the optimization are our proposed non-intersect and contact losses based on uniformly random points. For each row, we show the original positions of the hand and object in space (first column), and then three views of the optimized hand interacting with the object.

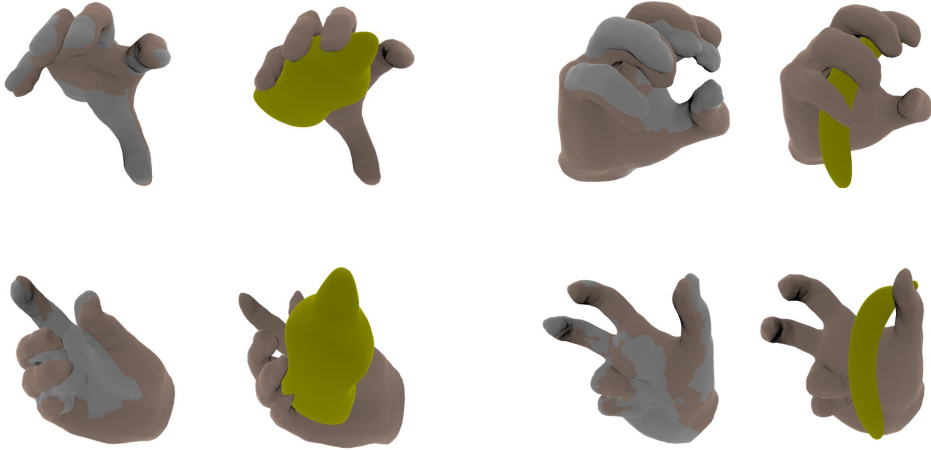


Figure 5: **Modifying Hand Poses.** We visualize how our losses optimize the hand shapes to have a better “grip” on objects. For each pair, we show the original hand pose (colored in gray) overlaid by the optimized hand pose (colored in the skin color), and how the optimized hand interacts with the object. As can be seen, the hand model moves the fingers to positions that increase the contact areas (top row) or to positions that do not intersect the objects (bottom row).

Further, the interaction between objects can be refined by choosing a set of points as anchors to modify the object surfaces. Experiments on 3D heart reconstruction and hand-object interaction demonstrate the effectiveness of our proposed method.

In general, our work highlights the importance of incorporating topological priors in 3D multiple-object reconstructions. By leveraging stochastic sampling, we enable accurate modeling of object interactions which is crucial in various domains. For example, topological priors can be applied to the reconstruction of skeletal structures since they are typically positioned in fixed relationships with each other. In robotics, we can incorporate topological priors that define the expected contact patterns and containment relationships to enhance the robot’s ability to manipulate objects accurately and with minimal collisions.

## A Enforcing Containment with Fixed Distances between Classes

In the main paper, we have presented our system to enforce two 3D objects to have a specific contact ratio. In general, our proposed concept of using random points to observe and manipulate the topological interaction between objects can be used for various types of topological constraints. In this section, we describe how we can enforce a containment relationship between two objects (one is completely inside the other) while also maintaining their surface distance within a specific range. This is particularly useful for modeling 3D objects with designated “thickness” attributes where the inner and outer layers are viewed as separate objects with the aforementioned topological interaction.

Let us consider two deep-SDF objects  $f_A(a, \cdot)$  and  $f_B(b, \cdot)$ . Our objective is to ensure that all points on the surface of  $f_B(b, \cdot)$  are located within the interior of  $f_A(a, \cdot)$  while the distance between them, *i.e.*, the thickness of the wall, is always in the range  $[\epsilon_{min}, \epsilon_{max}]$ . We assume that  $\epsilon_{min}$  and  $\epsilon_{max}$  are given or can be easily computed from the training data.

To achieve this, we begin by uniformly sampling  $N$  random points, denoted as  $x_i : i \in (1, N)$ . From this set, we select a set of points,  $\mathcal{A}$ , containing points that are in proximity (based on a predefined small threshold) to the surface of either object.

To ensure that  $f_B(b, \cdot)$  is strictly located inside  $f_A(a, \cdot)$ , we can minimize the following containment loss that penalizes points located outside  $f_B(b, \cdot)$  but inside  $f_A(a, \cdot)$ :

$$\mathcal{L}_{containment} = \sum_{x \in \mathcal{A}: (f_A(a, x) < 0) \wedge (f_B(b, x) > 0)} (-\text{clamp}(f_A(a, x), \delta_1) + \text{clamp}(f_B(b, x), \delta_1)) \quad (9)$$

where  $\text{clamp}(\cdot, \delta)$  function restricts a given value between an upper and lower bound  $[-\delta, \delta]$  and  $\delta$  are hyper-parameters of our model. This loss drives the surfaces of both  $f_A(a, \cdot)$  and  $f_B(b, \cdot)$  toward the anchor points (see Fig.6a).

To ensure that the distance between two objects is in the range  $[\epsilon_{min}, \epsilon_{max}]$ , we first find anchor points lying on the areas where the local surface distance between the two objects is smaller than  $\epsilon_{min}$  or larger than  $\epsilon_{max}$ . Given a random point  $x$  that either locates ① inside both objects, ② between the two objects, or ③ outside both objects, we can estimate the length  $d$  of a line segment lying between a pair of two objects  $(A, B)$  and passing through  $x$  as follow:

$$d = \text{sdf}(B, x) - \text{sdf}(A, x) \quad (10)$$

Based on this method to measure local surface distances, we select a set of points lying in areas where the distance between two objects is smaller than  $\epsilon_{min}$  and adjust the object surfaces by minimizing the following loss function, which increases the margin between the two objects:

$$\mathcal{L}_{pushing} = \sum_{x \in \mathcal{A}: (f_B(b, x) - f_A(a, x) < \epsilon_{min})} (\text{clamp}(f_A(a, x), \delta_2) - \text{clamp}(f_B(b, x), \delta_2)) \quad (11)$$

Similarly, we enforce a loss function with an opposite effect for points lying on areas where the distance between the two objects is larger than  $\epsilon_{max}$ :

$$\mathcal{L}_{pulling} = \sum_{x \in \mathcal{A}: (f_B(b, x) - f_A(a, x) > \epsilon_{max})} (-\text{clamp}(f_A(a, x), \delta_3) + \text{clamp}(f_B(b, x), \delta_3)) \quad (12)$$

The loss function to fine-tune the deep-SDFs of the two objects is:

$$\mathcal{L} = \mathcal{L}_{containment} \times \lambda_{containment} + \mathcal{L}_{pushing} \times \lambda_{pushing} + \mathcal{L}_{pulling} \times \lambda_{pulling} + \mathcal{L}_{data} \times \lambda_{data} \quad (13)$$

where  $\mathcal{L}_{data}$  is the data reconstruction term that regresses the signed distances[19] and  $\lambda$  are controlling parameters.

### A.1 Experiment

To demonstrate the effectiveness of this method, we conduct an experiment on reconstructing the *pseudo* inner walls of different heart components. We start from the occupancy matrix of each heart

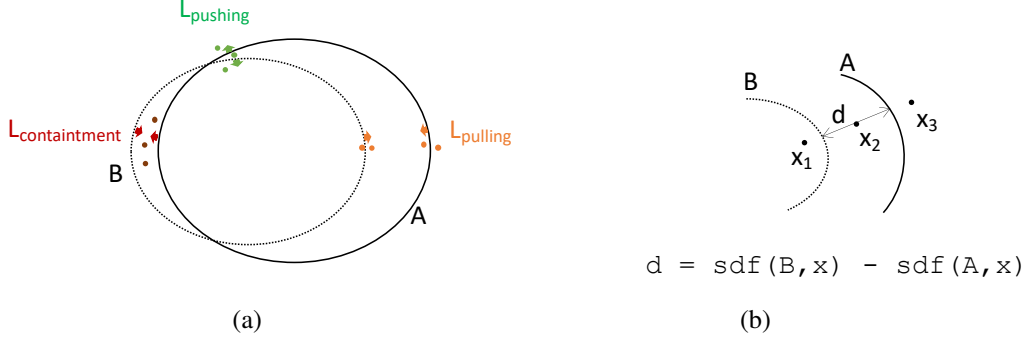


Figure 6: **Enforcing containment relationship with a minimum distance.** (a) We design losses to ensure that one object contains the other while maintaining a fixed distance between them. The local surface distance can be measured via signed distances from the two objects to an arbitrary point (b).

component and apply a 3D erosion operation to obtain an inner structure of each part. In this context, we consider the original structure as the “outer layer” and the eroded one as the “inner layer”, which are colored blue and yellow respectively in Fig. 7.

We use our proposed method to simultaneously model the outer and inner structures. In this experiment, we assume  $[\epsilon_{min} = 0.01, \epsilon_{max} = 0.03]$  are given (all vertex coordinates are scaled to  $[-1, 1]$  before training,  $[0.01, 0.03]$  is equivalent to  $[1.3, 3.8]$  pixels when rendering objects at size  $256^3$ ). Note that these values are specific to this proof-of-concept experiment and can be directly inferred from the erosion kernel.

For each pair of outer-inner objects, we sample 20000 points and their SDF values. We optimize the latent codes of two deep SDF models to fit these values. We compare a basic baseline trained with just the data term and our proposed method trained with the aforementioned loss functions. To evaluate the effectiveness of the methods, we measure the percentage of the inner object surface that violates the imposed topological constraints for each reconstructed outer-inner object pair. The summarized results are presented in Table 3. The baseline deepSDF model exhibits a violation rate of around 2-3% on the inner object surface, while our proposed method shows minimal violations.

We visualize an example in Fig.7. Both the baseline deepSDF [19] and our method can reconstruct the overall shapes of objects. However, in the last column, we highlight an area where the baseline deepSDF model exhibits a violation by reconstructing a partial surface of the inner object outside the outer object. Our method shows no violation. Additionally, we provide several examples of 2D slices from different objects in Fig.8. These examples demonstrate various cases where the baseline deepSDF model fails to generate objects that satisfy the imposed constraints. Our method show no violation in all cases.

Table 3: **Reconstructing outer-inner objects.** The inner object surface is expected to be within a distance range of 0.01 – 0.03 units from the outer object surface. With the baseline deepSDF model, approximately 2-3% of the inner object surface violates these constraints. In contrast, our proposed method demonstrates minimal to no violation.

Component	Violation (% area)		Violation (N.o. vertexes)		N.o. vertexes
	deepSDF	Ours	deepSDF	Ours	
MLV	3.51	0.11	4638.94	145.80	132104.5
LA	2.66	0.00	1170.26	0.00	43932.0
LV	3.36	0.00	2020.36	0.00	60126.6
RA	3.49	0.15	1267.76	55.66	36288.4
RV	2.31	0.02	1547.81	16.59	67140.2

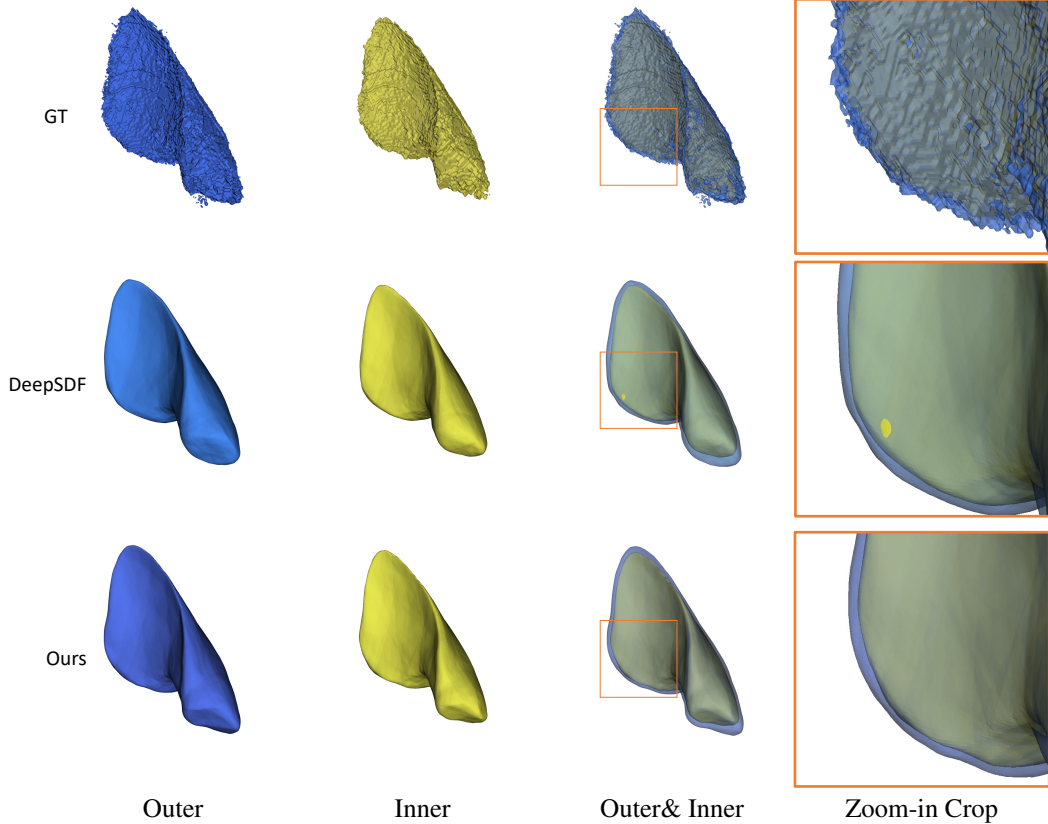


Figure 7: **Reconstructing a pair of outer-inner objects.** Both the baseline method deepSDF [19] and our method can accurately reconstruct the overall shapes of objects. The last column highlights an area where a partial surface of the inner object reconstructed by deepSDF is outside the outer object. There is no violation in our case.

## B More Details on Network Architecture and Optimization

In all of our experiments, we adopt the auto-decoder framework introduced in deepSDF [19]. The decoder network consists of 6 fully connected layers, each with 256 dimensions and ReLU activation. We utilize a Tanh activation function as the final layer to output the signed distance function (SDF) values. Layer normalization [?] is applied to normalize intermediate outputs after each layer. The auto-decoder is trained for 20,000 epochs using the Adam optimizer [?].

To prepare data, we normalize the vertices of each mesh to the range of  $[-1, 1]$ . For training, we sample 440,000 spatial points to compute SDF values for each shape. The ratio of points near the object’s surface to random points is set to 10:1. Throughout the optimization process, we sample 22,000 spatial points to compute SDF values for each shape. The baseline deepSDF models are trained for 20,000 epochs. It is important to note that while we use as input a small number of spatial points and their SDF values, the core idea of our method is independent of the input representation. Alternative approaches, such as training a 3D segmentation model to generate initial object meshes or training an encoder-decoder system to regress latent codes before refining them with our proposed method, can also be employed.

To refine the topological interaction, we uniformly sample 1M random points after every 200 iterations for heart component reconstruction and after every 20 iterations for hand-object reconstruction. Computing SDF distances from these points to deepSDF models requires a single feed-forward pass through each model and obtaining anchor points takes 0.1 seconds in total. For a pair of testing objects, we optimize the system for 2000 iterations, which takes 24 seconds for an NVIDIA A100 GPU. The baseline deepSDF takes 12 seconds.

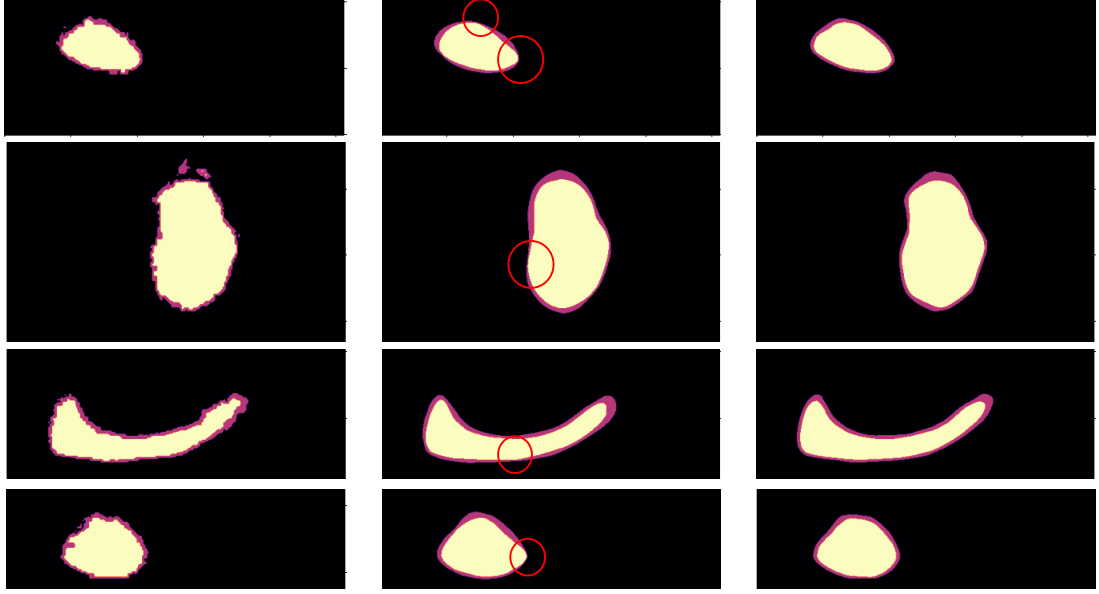


Figure 8: **Reconstructing a pair of outer-inner objects.** We aim to reconstruct a pair of outer-inner objects where the distance between them is in a fixed range. We visualize several cases where a baseline deepSDF model fails to generate objects that satisfy this constraint (circled in red). Our method works well in all cases.

We experimentally set the parameters  $(\delta_1, \delta_2, \delta_3)$  to  $(0.0001, 0.0001, 0.0001)$ . The parameters  $(\lambda_{ni}, \lambda_{contact}, \lambda_{non-contact}, \lambda_{data})$  in eq. (7) and  $(\lambda_{containment}, \lambda_{pushing}, \lambda_{pulling}, \lambda_{data})$  in eq. (13) are both set to  $(1, 1, 1, 5)$ .

### C Signed Distance Histogram Distance

To measure the topological similarities between two interactions, we propose the use of signed distance histogram distances. The histogram is computed by dividing the range of signed distances  $([-1, 1]$  in our paper) into bins and then counting the percentage of surface area that falls into each bin. The histogram considers both the intersection ratio (at bin “<0”) and the contact ratio (the smallest positive bin). We set the bin values at  $[-\infty, 0, 0.008, 0.08, 0.8, \infty]$  since all meshes are rendered to the size of  $256^3$  while the signed distances range from -1 to 1.

We visualize a few histograms computed between human heart components in Fig.9. In all cases, the histogram is computed for signed distances from the “green” object to the “orange” object. In the first column, we visualize the histograms computed for pairs of ground-truth objects. We then translate the “green” objects by a small offset of +3 and -3 pixels along the x-axis, which results in the middle and last columns, respectively. As can be seen, moving the objects by small offsets significantly change the topological interactions between them, *e.g.*, from contact with a large ratio to significantly intersecting. These variations in interactions are effectively captured and reflected in the computed histograms.

### D Hand contacting objects

We use our proposed losses with random anchor points to enforce a hand model to contact an arbitrary object. We first uniformly random 1 million spatial points and compute the signed distances from them to the deepSDF hand and object models. We then choose the top  $k\%$  of points lying close to the surface of the hand and enforce these points to be in contact distance with the object. We vary the value of  $k$  (10/20/30) as well as randomly initialize the pose, position, and rotating angle of the hand to obtain different hand-object interactions. It is important to note that not all latent embeddings

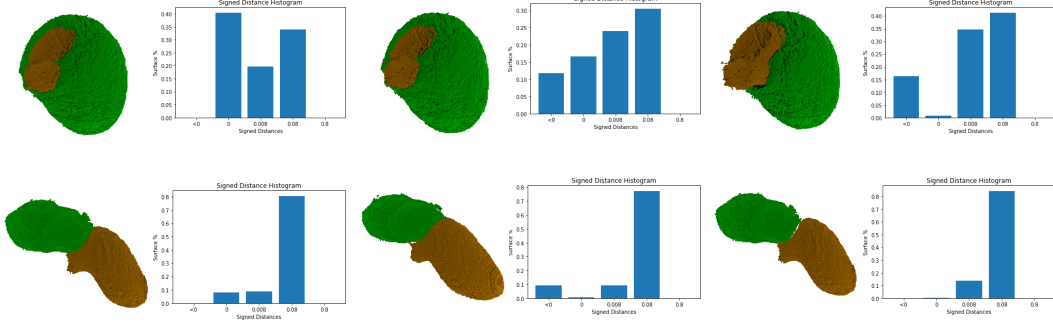


Figure 9: **Visualization of Signed Distance Histograms.** In all cases, the histogram is computed for signed distances from the “green” object to the “orange” object. In the first column, we visualize the histograms computed for pairs of ground-truth objects. We then translate the “green” objects by a small offset of +3 and -3 pixels along the x-axis, which results in the middle and last columns, respectively. As can be seen, moving the objects by small offsets significantly change the topological interactions between objects, which are reflected in the histograms.



Figure 10: **Interpolating between latent pose.** The first and last columns are hands generated from latent codes of training instances. The remaining hands are generated from the interpolated latent codes. Not all latent codes result in realistic hands.

result in realistic hands due to the limited training data. In some cases, the generated hand models may not appear visually realistic, as depicted in Fig. 10.

Different values of  $k$  lead to different interactions between the hand and the object. As the value of  $k$  increases, it encourages the hand model to find a position and pose that results in a larger contact ratio with the object. This effect is demonstrated in Figure 11 for two different objects. In each case, the model is initialized from the same pose and starting position, but as  $k$  increases, the hand “grasps” the objects differently, with increasing contact ratios from the top to bottom rows.

Our method enables the generation of diverse interactions between the hand model and any arbitrary 3D object, as illustrated in Figure 12. It is important to note that we do not explicitly control the location of the contact. Instead, the hand model autonomously determines where the contact occurs based on the optimization process. To avoid generating unrealistic hand shapes, such as those highlighted in the red bounding box, we utilize a small learning rate ( $1e-6$ ) for the latent code of the hand model. This helps to maintain the overall realism and stability of the generated hand-object interactions.

## E Visualizing Anchor Points

We visualize anchor points used in our method for refining interactions between different pairs of hand components. We choose among randomly sampled points ones that are close to the surfaces of both objects where the numbers of points are determined via a prior contact ratio. As can be seen, those anchor points are distributed evenly on the contact surface, allowing us to refine the interactions between the two objects.

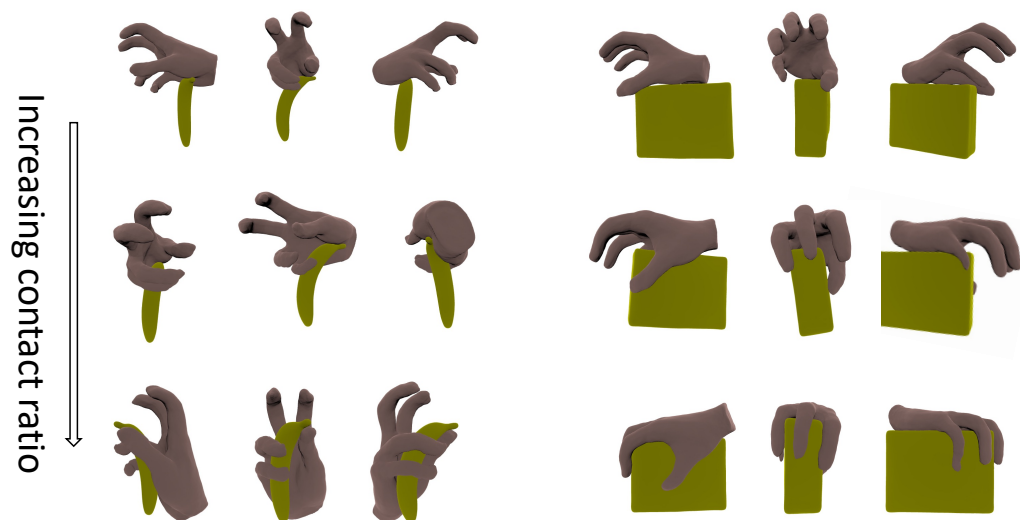


Figure 11: **Increasing the prior contact ratio.** As the value of the prior contact ratio ( $k$ ) increases, it encourages the hand model to find a position and pose that results in a larger contact ratio with the object. In each case, the model is initialized from the same pose and starting position, but as  $k$  increases, the hand "grasps" the objects differently, with increasing contact ratios from the top to bottom rows.





Figure 12: **Different hand-object interactions simulated via our method.** Our method can be used to obtain various interactions between the hand model and an arbitrary 3D object. We do not control where the contact takes place. We choose a small learning rate (i.e.,  $1e-6$ ) for the latent code of the hand model to avoid unrealistic hand shapes such as the ones highlighted in the red bounding box.

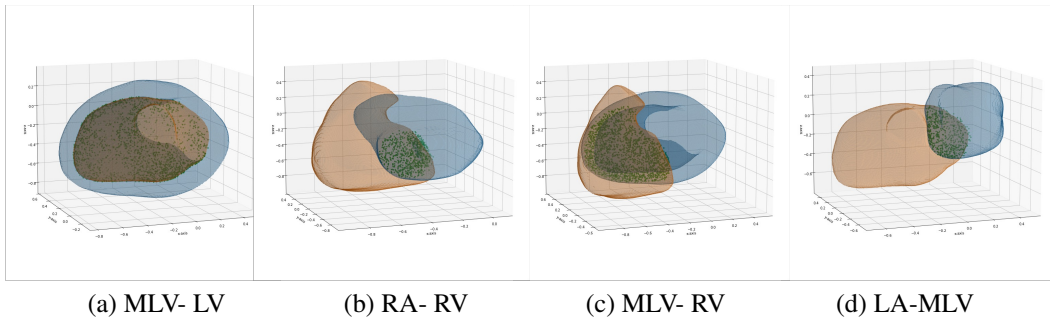


Figure 13: **Anchor points for refining the interactions between heart components.** We choose among randomly sampled points ones that are close to the surfaces of both objects where the numbers of points are determined via a prior contact ratio.



## References

- [1] Luca De Luigi, Ren Li, Benoit Guillard, Mathieu Salzmann, and Pascal Fua. DrapeNet: Garment Generation and Self-Supervised Draping. In *Proceedings of the IEEE/CVF Conference on Computer Vision and Pattern Recognition*, 2023.
- [2] Francis Engelmann, Konstantinos Rematas, B. Leibe, and Vittorio Ferrari. From points to multi-object 3d reconstruction. *2021 IEEE/CVF Conference on Computer Vision and Pattern Recognition (CVPR)*, pages 4586–4595, 2020.
- [3] G. Gkioxari, J. Johnson, and J. Malik. Mesh r-cnn. In *2019 IEEE/CVF International Conference on Computer Vision (ICCV)*, pages 9784–9794, 2019.
- [4] Saumya Gupta, Xiaoling Hu, James Kaan, Michael Jin, Mutshipay Mpoy, Katherine Chung, Gagandeep Singh, Mary Saltz, Tahsin Kurc, Joel Saltz, et al. Learning topological interactions for multi-class medical image segmentation. In *ECCV*, pages 701–718. Springer, 2022.
- [5] Shreyas Hampali, Mahdi Rad, Markus Oberweger, and Vincent Lepetit. Honnotate: A method for 3d annotation of hand and object poses. In *CVPR*, 2020.
- [6] Mohamed Hassan, Partha Ghosh, J. Tesch, Dimitrios Tzionas, and Michael J. Black. Populating 3d scenes by learning human-scene interaction. *2021 IEEE/CVF Conference on Computer Vision and Pattern Recognition (CVPR)*, pages 14703–14713, 2020.
- [7] Kaiming He, Georgia Gkioxari, Piotr Dollar, and Ross Girshick. Mask r-cnn. In *Proceedings of the IEEE International Conference on Computer Vision (ICCV)*, Oct 2017.
- [8] Xiaoling Hu. Structure-aware image segmentation with homotopy warping. 2021.
- [9] Xiaoling Hu, Fuxin Li, Dimitris Samaras, and Chao Chen. Topology-preserving deep image segmentation. In H. Wallach, H. Larochelle, A. Beygelzimer, F. d'Alché-Buc, E. Fox, and R. Garnett, editors, *Advances in Neural Information Processing Systems*, volume 32. Curran Associates, Inc., 2019. URL [https://proceedings.neurips.cc/paper\\_files/paper/2019/file/2d95666e2649fcfc6e3af75e09f5adb9-Paper.pdf](https://proceedings.neurips.cc/paper_files/paper/2019/file/2d95666e2649fcfc6e3af75e09f5adb9-Paper.pdf).
- [10] Muhammad Zubair Irshad, Thomas Kollar, Michael Laskey, Kevin Stone, and Zsolt Kira. Centersnap: Single-shot multi-object 3d shape reconstruction and categorical 6d pose and size estimation. *2022 International Conference on Robotics and Automation (ICRA)*, pages 10632–10640, 2022.
- [11] Muhammad Zubair Irshad, Sergey Zakharov, Rares Ambrus, Thomas Kollar, Zsolt Kira, and Adrien Gaidon. Shapo: Implicit representations for multi object shape appearance and pose optimization. 2022. URL <https://arxiv.org/abs/2207.13691>.
- [12] Korrawe Karunratanakul, Jinlong Yang, Yan Zhang, Michael J Black, Krikamol Muandet, and Siyu Tang. Grasping field: Learning implicit representations for human grasps. In *2020 International Conference on 3D Vision (3DV)*, pages 333–344. IEEE, 2020.
- [13] Haoming Li, Xinzhuo Lin, Yang Zhou, Xiang Li, Yuchi Huo, Jiming Chen, and Qi Ye. Contact2grasp: 3d grasp synthesis via hand-object contact constraint, 2023.
- [14] Feng Liu and Xiaoming Liu. Voxel-based 3d detection and reconstruction of multiple objects from a single image. In *Neural Information Processing Systems*, 2021.
- [15] William E. Lorensen and Harvey E. Cline. Marching cubes: A high resolution 3d surface construction algorithm. *Proceedings of the 14th annual conference on Computer graphics and interactive techniques*, 1987.
- [16] Qianli Ma, Jinlong Yang, Anurag Ranjan, Sergi Pujades, Gerard Pons-Moll, Siyu Tang, and Michael J. Black. Learning to dress 3d people in generative clothing. In *Proceedings of the IEEE/CVF Conference on Computer Vision and Pattern Recognition (CVPR)*, June 2020.
- [17] Agata Mosinska, Pablo Márquez-Neila, Mateusz Koziński, and P. Fua. Beyond the pixel-wise loss for topology-aware delineation. *2018 IEEE/CVF Conference on Computer Vision and Pattern Recognition*, pages 3136–3145, 2017.

- [18] Yinyu Nie, Xiaoguang Han, Shihui Guo, Yujian Zheng, Jian Chang, and Jian Jun Zhang. Total3dunderstanding: Joint layout, object pose and mesh reconstruction for indoor scenes from a single image. In *IEEE/CVF Conference on Computer Vision and Pattern Recognition (CVPR)*, June 2020.
- [19] Jeong Joon Park, Peter R. Florence, Julian Straub, Richard A. Newcombe, and S. Lovegrove. DeepSDF: Learning continuous signed distance functions for shape representation. *2019 IEEE/CVF Conference on Computer Vision and Pattern Recognition (CVPR)*, pages 165–174, 2019.
- [20] Javier Romero, Dimitrios Tzionas, and Michael J. Black. Embodied hands. *ACM Transactions on Graphics (TOG)*, 36:1 – 17, 2017.
- [21] Yufei Ye, Abhinav Kumar Gupta, and Shubham Tulsiani. What’s in your hands? 3d reconstruction of generic objects in hands. *2022 IEEE/CVF Conference on Computer Vision and Pattern Recognition (CVPR)*, pages 3885–3895, 2022.
- [22] Xiahai Zhuang and Juan Shen. Multi-scale patch and multi-modality atlases for whole heart segmentation of mri. *Medical image analysis*, 31:77–87, 2016.